Development of Modeling of Differential Shrinkage Effect on Jointed Concrete Pavements for Korean Pavements Design

Jin-Sun Lim*, Jin-Hoon Jeong, Ren-Juan Sun***, Dan G. Zollinger******

**** Graduate Student, Department of Civil Engineering, Inha University,***
253 Yonghyeon-dong, Nam-gu, Incheon 402-751, South Korea
coreplay@hanmail.net

ABSTRACT

The non-uniform moisture distribution through the depth of jointed concrete pavement (JCP) causes greater shrinkage at the top of the slab rather than at the bottom. This kind of shrinkage behavior induces warping and tensile stress in the top surface of slab. The warping shape changes with concrete age. In this study, an instrumented concrete slab with vibrating strain gauges was constructed in the field to investigate temperature-induced strains in the slab, the coefficient of thermal expansion (CTE) of concrete was tested in laboratory, and the thermal and shrinkage strains were analyzed. In addition, shrinkage of the concrete slab was predicted via the ACI (American Concrete Institute) 209R-92 Code. The relevant correction factors were determined by simultaneous equations for different vertical positions. The shrinkage effects on the pavement slab were converted to thermal effects and shrinkage-equivalent temperature difference (SETD) was used to quantify the effects of shrinkage on behavior of the concrete pavement.

1. INTRODUCTION

Various researchers have carried out extensive work to quantify and predict the effects of shrinkage on the pavement slab exposed in natural environment. During the 1930's, extensive studies were conducted by the Bureau of Public Roads of America to evaluate the effects of variations in moisture on the behavior of concrete slab. In late 1980's, Jansen concluded from the results of field test, laboratory test, and computer modeling that nonlinear shrinkage occurred throughout the slab thickness, which acted in a manner similar to what the nonlinear temperature distribution did *[2]*. Based on the result, Eisenmann and Leykauf developed a model calculating slab curling due to the shrinkage of slab surface *[3]*. The moment due to the surface shrinkage could be compared with the fictitious equivalent moment caused by a linear negative temperature gradient. Eventually, the model was adopted by the Mechanistic-Empirical Pavement Design Guide (MEPDG) in 2004 *[4]*. While the drying shrinkage occurs only near the slab surface, the model does not express long-term increase of the shrinkage difference between top and bottom of the slab reasonably. As the result, the shrinkage-equivalent temperature difference (SETD) calculated by the model shows only seasonal fluctuations

near 0 ℃.

Shrinkage is a complex phenomenon which is influenced by many factors including the concrete constituents, the temperature and relative humidity of the environment, and the size of the structure or member *[5]*. Hence, a major handicap has been in most of the early studies and even now, due to the lack of reliable techniques to measure concrete shrinkage in the field, there are some errors in field testing results. On the other hand, the prediction models for shrinkage can not express the difference of shrinkage at different location and depth within a specific concrete member. In this study, several existing prediction models are analyzed and ACI 209R-92 is selected to predict the shrinkage of a concrete pavement slab as shown in equation (1).

$$\varepsilon_{\mathrm{st}} = \frac{t}{T_c + t}\varepsilon_{su} \qquad (1)$$

where,

ε_{st} = shrinkage after t days since the end curing

t = time in days since the end of curing

T_c = 35 days for moisture curing (this study) and 55 days for steam curing

ε_{su} = ultimate shrinkage

2. TESTING PROCEDURES AND RESULTS

Of interest is the environmentally related effects on slab behaviors such as those directly related to moisture movement and temperature change of concrete independent of the slab action due to traffic loading. Hence, the shrinkage strain of slab can be gained by subtracting thermal strain from total strain of concrete. The instrumented slab was constructed in field to investigate the total strain behavior of the slab and CTE of concrete was tested in laboratory for shrinkage strain analysis.

2.1 Experiment of Strain in Field

To investigate the climatically related behavior of the pavement slab and joint, a two-lane experimental jointed plain concrete pavement (JPCP) section 152 m in length was constructed at Dangjin Gun, Korea on June 2, 2007. The 300 mm thick slabs with 6.0 m and 4.1 m in length and width were placed on a lean concrete base layer laying on compacted soil subgrade. After the placement, the concrete slab was cured using a curing compound. The mix design and characteristics of materials used in this testing was as shown in TABLE 1.

TABLE 1. Mix Design and Characteristics in 1 m^3 of Concrete

Materials	Cement	Fly ash	Water	Fine aggregate	Gravel	AD1	Slump	W/C	Air Content	S/A
Proportions	310 kg	55 kg	161 kg	700 kg	1078 kg	1.83 kg	10 mm	0.441	5±1 %	0.394

The strain gauges, temperature and moisture testing devices, i-buttons, dial gauges, and demac gauges were instrumented in a single slab to investigate the slab strains, the moisture and temperature distribution of concrete slab, vertical displacement of slab edge, and the joint behavior of the pavement, respectively. Eight vibrating wire strain gauges (Geokon Model VCE- 4200) were installed at 4 locations in the slab, two locations were the mid-slab edge positions transversely and longitudinally oriented, one was the slab corner and one was the center of the slab. They were placed in pairs at depths of 50 mm and 250 mm from the top surface of the slab. There were no dowel bars used but tie bars were installed along the transverse and longitudinal joints of the slab, respectively. The instrumentation is shown in FIGURE 1. After the placement of the concrete slab, the temperatures and strains were recorded from the readout equipment GK-401.

The data were collected in three stages after the placement, which was from June 2 to June 5, from October 24 (144 days after placement) to October 25 of 2007, and from April 14 to April 15 of 2008 (317 days after the placement), respectively. These three stages belonged to the summer, autumn and spring seasons of Korea. For the sake of brevity, the details of testing and analysis other than strains and temperatures

The strain gauges, temperature and moisture testing devices, i-buttons, dial gauges, and demac gauges were instrumented in a single slab to investigate the slab strains, the moisture and temperature distribution of concrete slab, vertical displacement of slab edge, and the joint behavior of the pavement, respectively. Eight vibrating wire strain gauges (Geokon Model VCE- 4200) were installed at 4 locations in the slab, two locations were the mid-slab edge positions transversely and longitudinally oriented, one was the slab corner and one was the center of the slab. They were placed in pairs at depths of 50 mm and 250 mm from the top surface of the slab. There were no dowel bars used but tie bars were installed along the transverse and longitudinal joints of the slab, respectively. The instrumentation is shown in FIGURE 1.

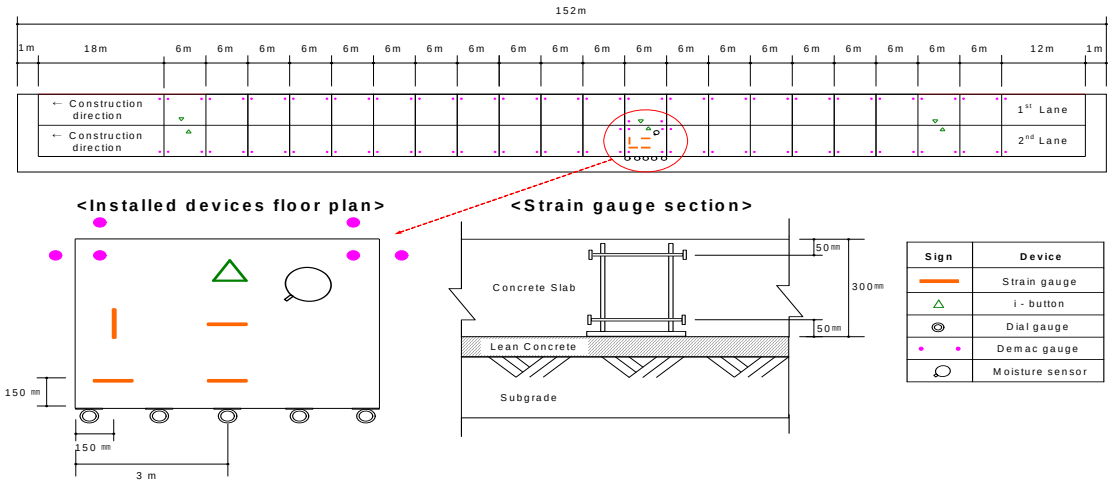

FIGURE 1. Layout of Slab Instrumentation

After the placement of the concrete slab, the temperatures and strains were recorded from the readout

equipment GK-401. The data were collected in three stages after the placement, which was from June 2 to June 5, from October 24 (144 days after placement) to October 25 of 2007, and from April 14 to April 15 of 2008 (317 days after the placement), respectively. These three stages belonged to the summer, autumn and spring seasons of Korea. For the sake of brevity, the details of testing and analysis other than strains and temperatures of slab are not presented here.

In addition, the ambient temperature and RH were monitored during the investigation stages for analytical purposes and the results were shown in FIGURE 2. Both temperature and RH show obvious cyclic trends in a 24-hour time period. The lowest temperature appears around 4:00 am in the morning and the highest temperature appears around 1:00 pm in the afternoon of everyday, but the RH shows an opposite character with that of temperature, which induces the minimum peak temperature corresponds to the maximum peak RH in the morning and the maximum peak temperature corresponds to the minimum peak RH in the afternoon.

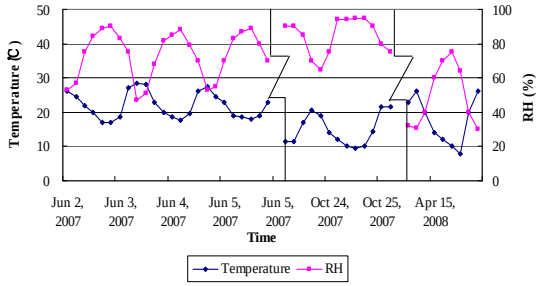

FIGURE 2. Ambient Temperature and RH during Investigation Period

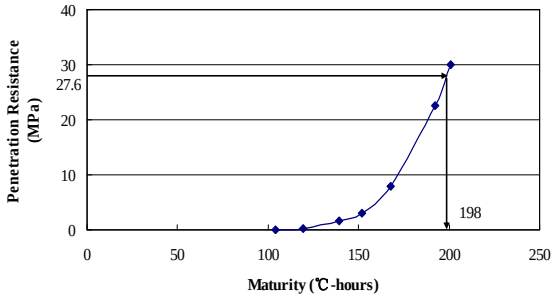

FIGURE 3. Maturity at Final Setting of Concrete

As we know, immediately after construction the concrete, slab maintained a level surface until curling and warping displacements were initiated. The maturity of final setting of the concrete slab was found using test procedure ASTM C 403 *(13)* to represent the initiation point of curling and warping. The maturities 198 ℃-hours was correlated with 27.6 MPa (final setting resistance) of penetration resistance, as shown in FIGURE 3. The final setting time was 5:00 pm which was 5 hours after placement of concrete. Testing data of the slab was analyzed from this time, when the strains of the slab began to change consistently at every position.

Although the strains investigated in field are total strains, the component strains consist of thermal and moisture effects. The investigated temperatures and total strains of the slab during three different stages are shown in FIGURE 4 and FIGURE 5, respectively.

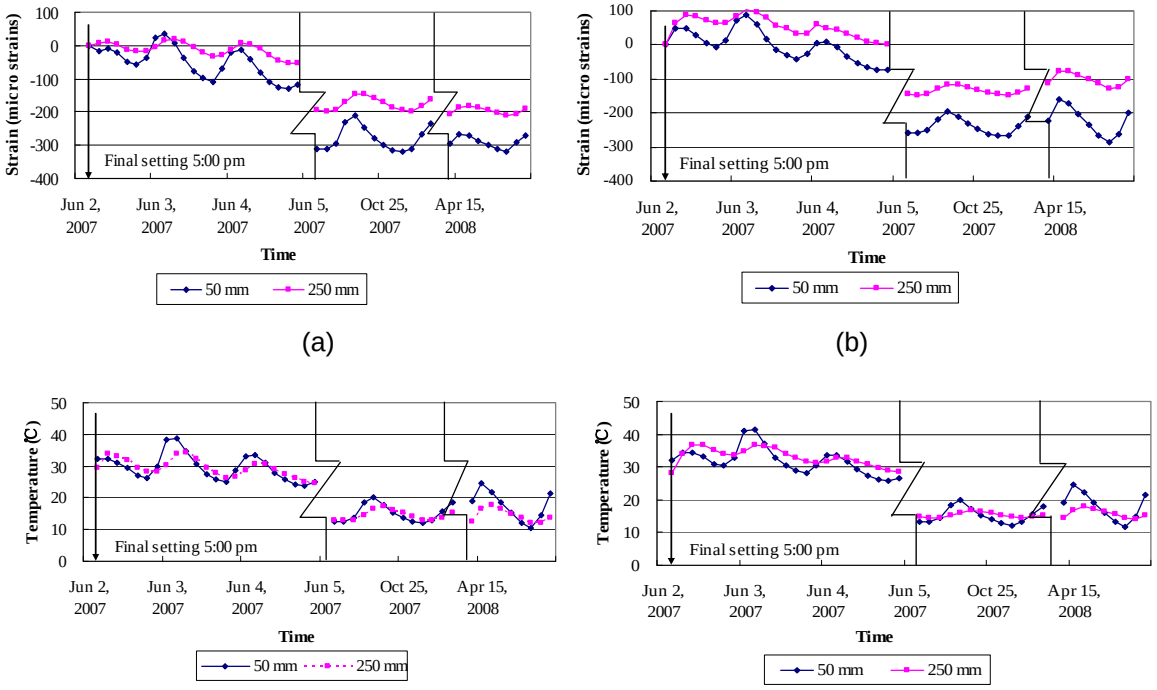

FIGURE 4. Temperature of Concrete Slab: (a) Corner of Slab; (b) Transverse Mid-Slab Edge; (c) Longitudinal Mid-Slab Edge; (d) Center of Slab

Apparently, during the very early stages of the life of the slab, the heat generation due to the hydration of the cement resulted in a temperature increase of the concrete slab which decreased later due to the effects of the ambient conditions. Slab temperatures peaked at 4:00 pm the day following placement, 28 hours after construction of the slab. The lowest temperature occurred at 7:00 am approximately 3 hours later than the ambient temperature cycle shown in FIGURE 2. In any case, the slab temperatures cycle over a 24 hour period. The temperature at a depth of 50 mm changes a little more than the temperature at 250 mm.

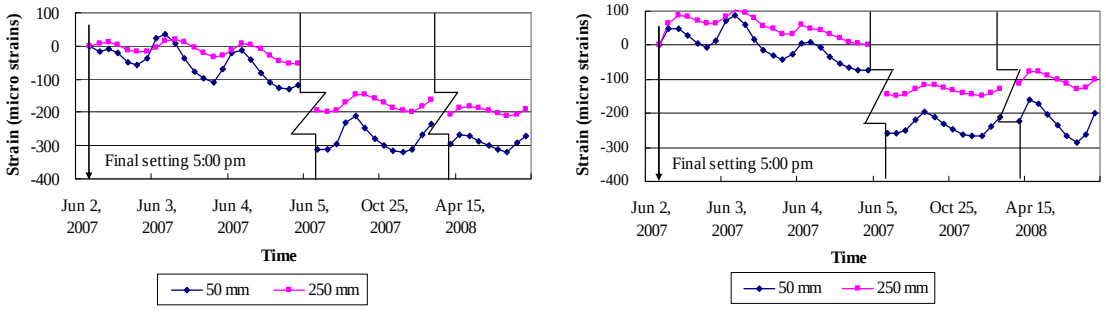

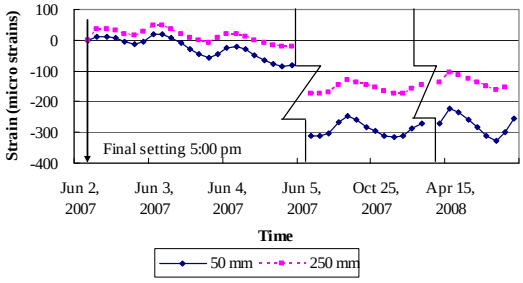

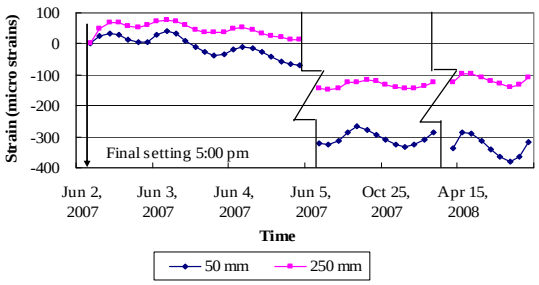

(c) (d)

FIGURE 5. Total Strain of Concrete Slab: (a) Corner of Slab; (b) Transverse Mid-Slab Edge; (c) Longitudinal Mid-Slab Edge; (d) Center of Slab

When the temperature of concrete increases from the final set temperature, the concrete began to expand, creating a tensile strain with depth. Thereafter, with the decrease of the temperature and the increase of drying shrinkage of concrete, tensile strains gradually changed to compression strains. The increase of the compressive strains at the top of the slab occurred earlier than those at bottom, hence, the strains at the top were larger than those at the bottom, which meant the slab almost maintained an upward curling configuration, which was not consistent with the small temperature difference between the top and the bottom of the slab as shown in FIGURE 2. This phenomenon suggests that the effects of shrinkage on the pavement shape are more crucial than those of temperature. In addition, the differences between top and bottom of the slab at different locations and time are not consistent creating a distortion of slabs warping and curling behavior, which is not consistent with the similar exhibition of temperature shown in FIGURE 4.

2.2 Thermal and Shrinkage Strain

Conventionally, total strain is the combination of strain due to sustained stress, creep, thermal and shrinkage strain. Thermal strain is calculated by multiplying CTE with the temperature difference between calculating time with final setting time. Hence, shrinkage strain should be the result of subtracting sustained strain, creep, and thermal strain from total strain. Because there was no sustained loading applied on the concrete slab during the testing stage, creep was ignored in this study.

In order to test the CTE of concrete, a test was carried out in laboratory according to AASHTO Provisional Standard TP 60 *[14]*. In this test, a concrete cylinder 100 mm in diameter and 200 mm in height was made and was installed on an invar frame as shown in FIGURE 6(a). The sample was then submersed under water in a temperature-controlled bath, water temperature was and cycled between 10 ℃ and 50 ℃; the length change measurements were made using of a submersible linear variable differential transformer (LVDT). The mix design and related material characteristics were the same as the field concrete shown in TABLE 1. The data collected from the laboratory were used to calculate the CTE from the slope of the length change versus temperature curve. Slope of the linear relationship

between these two variables is 9.41×10^{-6} /℃ assigned as the CTE of concrete as shown in FIGURE 6(b).

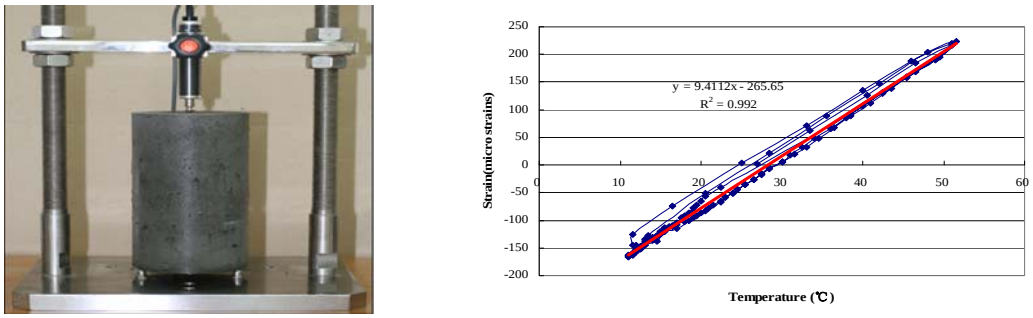

(a) (b)

FIGURE 6. Instrumentation of Concrete CTE Testing:
(a) Sample Installed on Invar Frame; (b) Ruselts of CTE Test
(b)

The relationship between total strain, thermal strain and shrinkage strain can be expressed in equation (2), (3) and (4).

$$\varepsilon_{Total} = \varepsilon_T + \varepsilon_{Sh} \quad (2)$$

$$\varepsilon_{Sh} = \varepsilon_{Total} - \varepsilon_T \quad (3)$$

$$\varepsilon_T = \alpha_T \Delta T \quad (4)$$

where,

ε_{Total} = total strain of slab
ε_T = thermal strain of slab
ε_{Sh} = shrinkage strain of slab
α_T = CTE of concrete
ΔT = temperature difference

The calculations of thermal strain and shrinkage strain were carried out according to equations (3) and (4) based on the experiment data. The results are shown in FIGURE 7. Both the thermal strains and shrinkage strains show daily cyclic changing character, which similarly correspond to the shift character of the environment factors shown in FIGURE 2, they change more at the top than at the bottom, which are the same as the total strains shown in FIGURE 5, but with some different appearance between thermal strains and shrinkage strains as shown in following paragraphs. All the thermal strains peak in the afternoon and reach their least value in the early morning, which correspond to the highest and lowest ambient and concrete temperatures as shown in FIGURE 2 and FIGURE 4, respectively. The shrinkage strains at the top of the slab peak in the early morning and reach a minimum value in the early morning, which approximately correspond to the highest and

lowest ambient RH as shown in FIGURE 2, but the shrinkage strains at the bottom of the slab don't show similar trends.

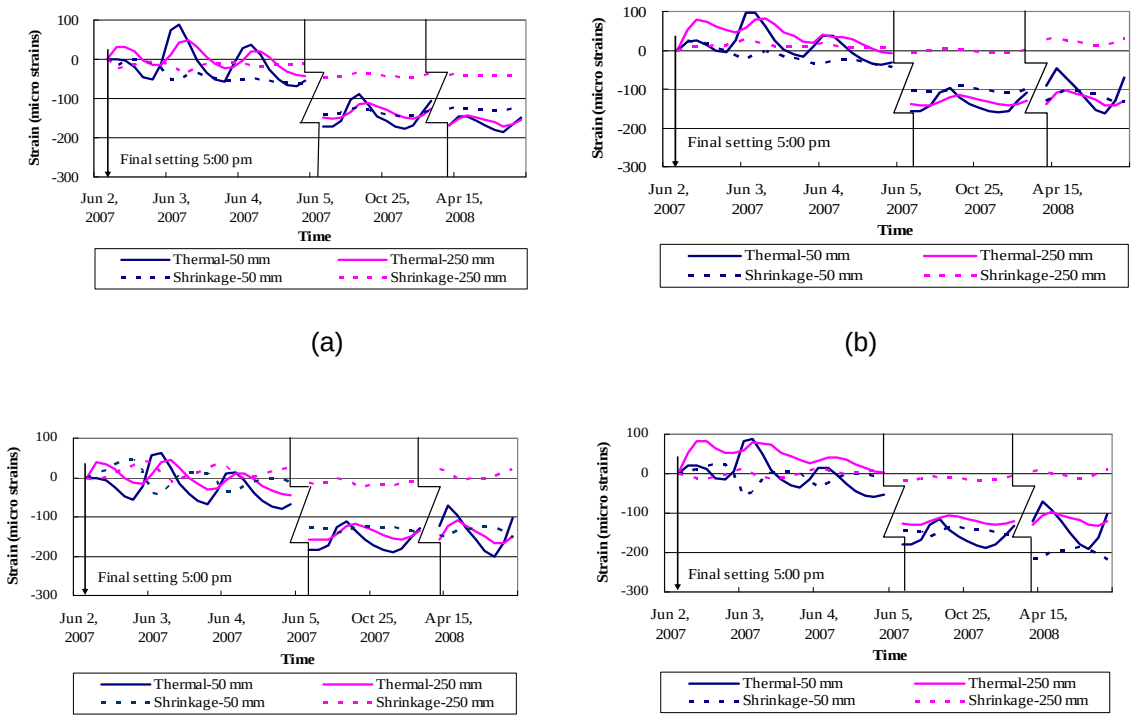

FIGURE 7. Thermal and Shrinkage Strain of Concrete Slab: (a) Corner of Slab; (b) Transverse Mid-Slab Edge; (c) Longitudinal Mid-Slab Edge; (d) Center of Slab

The thermal strain at the top and bottom of the slab change synchronously and the differences between them are small and there is no evident differences among the thermal strains at the four locations, which corresponds to the characteristics of the concrete temperatures shown in FIGURE 4. The shrinkage strains at the top of the slab increase continuously but change rarely at bottom; as a result, the differences between top and bottom increase gradually initially and then remain relatively stable thereafter. It is noted that the shrinkage strains at the bottom during the third stage are a little more than the strains during the second stage. This can be explained by two reasons; one pertains to the fact that there was rain two days before the measurements were made possibly affected by water accumulation between the slab and base; the other reason pertains to the large increase in warping induced strain at the slab bottom.

The shrinkage strain difference between top and bottom of the slab is largest at the slab center and smallest at the slab corner, which can be explained by that the effects of the environment and boundary conditions at the surface of the slab being similar at all locations, but those of the bottom are not. The daily shift range in thermal strains is larger than that occurs in the shrinkage strains. These phenomena show that the daily temperature effects on slab behavior are more significant than those due to shrinkage strain but shrinkage strain is the dominative factor in long-term slab behavior.

3. SHRINKAGE-EQUIVALENT TEMPERATURE DIFFERENCE

Shrinkage behavior of a concrete slab can be described relative to thermal behavior and as such slab shrinkage strains has been converted to thermal strains in this paper and this design strategy is also selected in MEPDG. The unique predicted shrinkage strain and CTE were used to calculate SETD. However, that model doesn't represent the shrinkage differences of different locations and depths, and the seasonal variations in ambient RH are oversimplified. The condition factors associated with the ACI 209R-92 model were corrected to better predict the shrinkage strain which were expressed in terms of temperature differences vertically through the slab termed as SETD.

3.1 Calculation of SETD

According to previous analysis, there are differences of shrinkage strain between different depths below the slab surface, and these differences can be calculated as shown in equation (5). The shrinkage behavior is similar as the thermal behavior in this regard, allowing the shrinkage strain to be converted to an equivalent thermal strain as shown in equation (6), which is related to the thermal property of the concrete and the temperature difference

$$\Delta\varepsilon_{Sh} = \Delta\varepsilon_{Total} - \Delta\varepsilon_{T} \quad (5)$$

$$\Delta\varepsilon_{\mathrm{Sh}} = \Delta\varepsilon_{Te} = \alpha_{T}\Delta T_{e} \quad (6)$$

where,

$\Delta\varepsilon_{\mathrm{Sh}}$ = shrinkage strain difference between different depths of slab

$\Delta\varepsilon_{Total}$ = total strain difference between different depths of slab

$\Delta\varepsilon_{T}$ = thermal strain difference between different depths of slab

$\Delta\varepsilon_{Te}$ = shrinkage equivalent thermal strain difference

ΔT_{e} = shrinkage equivalent temperature difference

So, SETD is:

$$\Delta T_{\mathrm{e}} = \frac{\Delta\varepsilon_{Sh}}{\alpha_{T}} \quad (7)$$

In order to study the strain differences between the top and bottom of the slab, the strains of top and bottom of the slab were determined by linear extrapolation between the strains measured at the 50 mm and 250 mm depth. The SETD of corner, transverse mid-slab edge, longitudinal mid-slab edge, and center of slab calculated according to equation (7) are shown in FIGURE 9 (a). A positive equivalent temperature difference refers to a higher equivalent temperature at the top of the slab than at the bottom of the slab and a negative value refers to the opposite.

In the early stage, the equivalent temperature difference increase from zero to a positive value,

which means the higher equivalent temperature occurs at the top than at the bottom causing the slab curls down. Then, with the development of the drying shrinkage of the concrete mostly occurring near the top of the slab, the equivalent temperature differences decreases to a negative value meaning a higher equivalent temperature at the slab bottom than at the top causing the slab to curl up. At later concrete ages, the equivalent temperature differences decrease to large negative values which mean greater curling up behavior occurs in the slab. In addition, obvious differences are among different locations of the slab which show that location effects can be represented by SETD analysis.

3.2 Modeling of SETD

The shrinkage strains investigated at different locations and depths within the pavement slab vary from point to point, but the shrinkage strains predicted by the existing models are sensitive to this aspect. Consequently ACI 209R-92 model was modified as shown below:

$$\varepsilon_{Sh} = C \times \varepsilon_{st} \qquad (8)$$

where, C is condition factor varying with the friction between slab and base layer, the presence of dowels and tie-bars, slab size, curing method, climatic condition, and so on. It can be defined as the linear formula as shown in equation (9) to be obtained by a regression analysis.

$$C = a \times z + b \qquad (9)$$

where,

z = vertical coordinate (mm), defined as zero at bottom surface

a, b = regression constants

a and b are obtained by the simultaneous equations (10) and (11).

$$(az_1 + b)\varepsilon_{st} = \varepsilon_{Sh1} \qquad (10)$$

$$(az_2 + b)\varepsilon_{st} = \varepsilon_{Sh2} \qquad (11)$$

z_1 and z_2 are the testing point coordinates 50 mm and 250 mm respectively, the corresponding shrinkage strains tested at the two points are designated as ε_{Sh1} and ε_{Sh2}, and the predicted shrinkage strains ε_{st} of concrete slab are calculated according to equation (1).

The regression constants of the four locations are illustrated in TABLE 2. Values of the constants relative to the four locations vary from location to location and this variation can distinguish the different locations in the following predicted SETD. The shrinkage strain differences between top and bottom of the slab at different locations can be calculated as below:

TABLE 2. Regression Constants of Concrete Slab

Locations	a	b
Corner	0.00389	0.08537
Transverse Mid-slab Edge	0.00418	-0.27981
Longitudinal Mid-slab Edge	0.00452	-0.19809
Center	0.00578	-0.24137

$$\Delta\varepsilon_{Sh} = \Delta C\varepsilon_{st} \qquad (12)$$

where, ΔC is difference of condition factor between top and bottom of slab($= C_{Top} - C_{Bottom}$).

Because $C_{Top} = ah + b$ and $C_{Bottom} = 0 + b$, $\Delta C = ah$ as previously noted, the SETD can be synthesized by equation (1), equation (7), and equation (12) and is expressed as equation (13).

$$\Delta T_e = \frac{\Delta\varepsilon_{sh}}{\alpha_T} = \frac{\Delta C\varepsilon_{st}}{\alpha_T} = \frac{ah\varepsilon_{st}}{\alpha_T} = \frac{ah}{\alpha_T}\left(\frac{t}{T_c + t}\right)\varepsilon_{su} \qquad (13)$$

where, h is thickness of concrete slab.

The SETD between top and bottom of slab is affected by regression constant a, slab thickness, prediction shrinkage strain and CTE of the concrete. The SETD predicted according to equation (13) is shown in FIGURE 8 (b). The SETD increases from zero gradually and becomes relatively stable after a period of time. There are some differences in the SETD among the four locations. The largest value of the regression constant a at the center of the slab corresponds to the largest value of SETD at the slab center and the smallest value of a at the slab corner corresponds to the largest value of SETD at the slab corner. The sequence from small to large is similar to the measured values shown in FIGURE 8 (a).

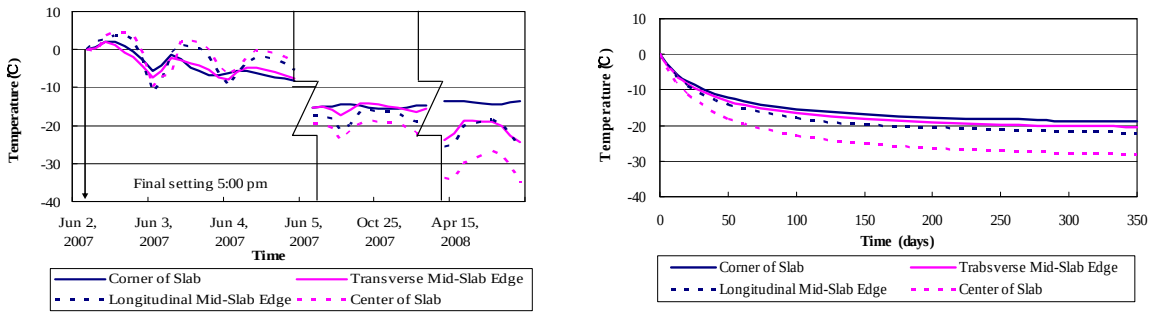

(a) (b)

FIGURE 8. SETD of Concrete Slab: (a) Measured SETD; (b) Predicted SETD

4. Verification of SETD

The strain data collected in an experiment in Texas A&M University *(15, 16)* were analyzed to verify the SETD modeling. A slab instrumented with experimental devices was constructed at the Riverside Campus of Texas A&M University on August 4, 2000. The construction consisted of the 305 mm slab with 9.1 m and 3.7 m in length and width. The concrete slab placement was cured in two halves where the 1st half was placed at 10:15 am and cured with a 13 mm insulated mat, the 2nd half was placed at 12:00 pm was cured with a single coat of a water base Type Ⅱ Class A curing compound. The final setting time was 3:30 pm and 5:00 pm, respectively by correlating to ASTM C 403. The dowel bars were installed along the transverse joint between the two halves. Six vibrating strain gauges were installed at the undoweled transverse mid-slab edge, longitudinal mid-slab edge, and center of slab, in pairs at a depth of 25 mm and 279 mm. The data were collected in several stages over a 1 month period for the insulated mat curing half and over 2 years for the curing compound curing half after the construction. The data of insulated mat curing half is not included in this paper.

The 2 year measurements were performed between late July and early September and ambient temperature during the periods were similar. The total strains of slab over two years were shown in FIGURE 10 and they show similar changing trend with that of Dangjin testing shown in FIGURE 5. After the placement of slab, both strains of top and bottom decrease gradually. The top strains decrease at a greater rate than those of the bottom, which result in a larger compressive strain at the top than at the bottom leading to a curled up shape of the slab. But the largest strain difference between top and bottom of slab appeared at the transverse mid-slab edge and lowest value appeared at the longitudinal mid-slab edge. The phenomenon is not same as that shown in FIGURE 4, which may be due to the different boundary conditions associated with the two slabs.

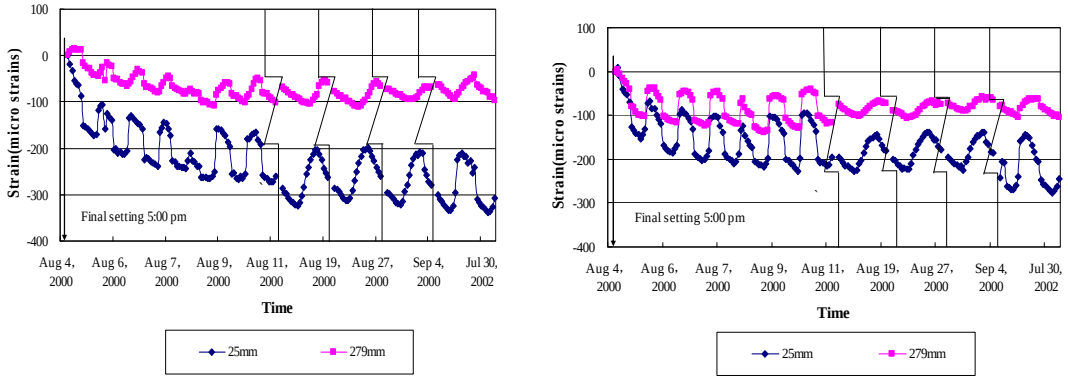

FIGURE 9. Total Strain of Test Slab for Verification: (a) Transverse Mid-Slab Edge; (b) Center of Slab

The thermal and shrinkage strains were calculated according to equation (3) and (4), and the results are shown in FIGURE 9. Similarly as shown in FIGURE 7, the thermal and shrinkage strains

shift daily. The range of thermal strain at the top is larger than at the bottom, which induces some thermal induced distortion between top and bottom. There is no evidence of differences in thermal strains among the three locations as well. Shrinkage strains at the bottom of slab slightly increase for all the locations, but those of top increase gradually to a large value after a long period of time, which is the main factor resulting in a warp up slab. There is evidence of differences in shrinkage strains among the three locations.

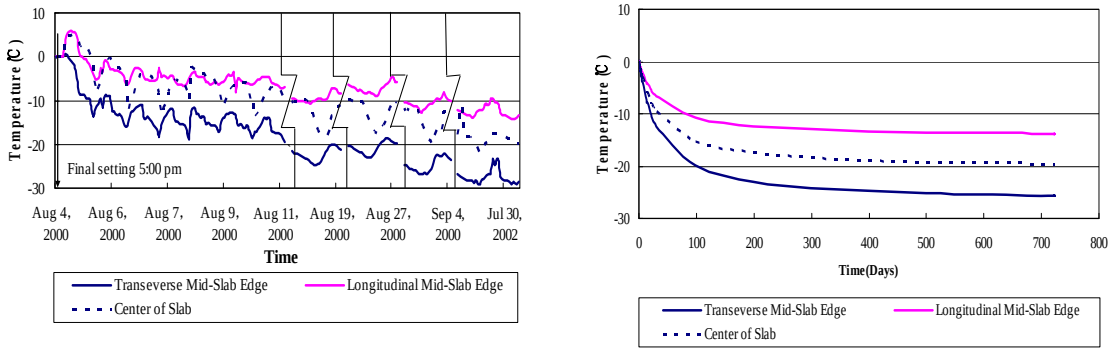

(a) (b)

FIGURE 10. SETD of Test Slab for Verification: (a) Measured SETD; (b) Predicted SETD

The measured SETD is shown in FIGURE 10 (a). The SETD used for verification purposes gradually decreased from zero to a relative stable negative value. The largest value appears at the transverse mid-slab edge of the slab and the smallest value appears at the longitudinal mid-slab edge. A similar analysis as previously noted of the combination of factors where the regression constants of different locations are shown in TABLE 3. The constants at different locations are different also. The predicted SETD was calculated according to equation (13) and the results are illustrated in FIGURE 12 (b). The result shows a similar increasing trend with that result shown in FIGURE 8 (b). The sequence from small to large is longitudinal mid-slab edge, center of slab, and transverse-mid slab edge, which is different with the previous analyzed result shown in FIGURE 7 (b). This may be again due to the different boundary conditions of the two experiments.

TABLE 3. Regression Constants of Test Slab for Verification

Locations	a	b
Transverse Mid-slab Edge	0.00542	-0.11106
Longitudinal Mid-slab Edge	0.00292	0.16537
Center	0.00415	0.11438

The results of the verification analysis suggest that the shrinkage equivalent temperature difference modeling can be used to predict the SETD of pavement slab, and that the condition factors effectively express the different behaviors occurring at the different locations.

5. CONCLUSIONS

The effects of shrinkage of concrete on shape and behavior of JPCP are prominent. Existing prediction models of shrinkage of concrete were reviewed and ACI 209 R-92 was selected to predict drying shrinkage strain over the early age of a concrete pavement. Tests of concrete for CTE and measures of slab strains were conducted in the laboratory and the field, respectively. The strain under the influence of environment changes gradually change with time and cycle daily over a 24-hour period, which result in upward curling of the slab. Shrinkage strain differences between the top and bottom of the slab are larger than the thermal strains. In other words, the SETD is larger than the pure temperature difference. The relevant correction factors are analyzed using the measured strains and the ACI 209 R-92 model predicted strains. The verification analysis confirmed the rationality of this modeling approach. Several different kinds of boundary conditions, environment factors, and location effects are important in the study of the condition factors. Further experimental evaluations and investigation terms are recommended for more insight in the future.

ACKNOWLEDGMENT

The research in this paper was sponsored by the Korea Research Foundation (KRF), the Ministry of Land, Transport and Maritime Affairs (MLTMA) of Korea and the Federal Highway Administration (FHWA) of U.S. The authors thank them for their financial supports.

REFERENCES

1. Rajeev, G., Ram, K., and Paul. D.K. “Comparative Study of Various Creep and Shrinkage Prediction Models for Concrete.” *Journal of Materials in Civil Engineering*, ASCE, Vol. 19, No. 3, Mar. 2007, pp. 249-260.
2. Janssen D. J. “Moisture in Portland Cement Concrete.” *Transportation Research Record 1121*, Transportation Research Board, Washington, D.C, 1987, pp. 40-44.
3. Eisenmann, J. and Leykauf, G. “Simplified Calculation Method of Slab Curling Caused by Surface Shrinkage.” *Proceedings, 2nd International Workshop on the Theoretical Design of Concrete Pavements,* Siguenza, Spain, 1990, pp. 185-197.
4. NCHRP. *Guide for Mechanistic –Empirical Design of New and Rehabilitated Pavement Structures.* Final Report. National Cooperative Highway Research Program, Transportation Research Board, Washington, DC, 2004.
5. Barr, B., Hoseinian, S.B., and Beygi, M.A. “Shrinkage of Concrete Stored in Natural Environments.” *Cement and Concrete Composites,* Vol. 25, No. 1, Jan. 2003, pp. 19-29
6. Mehta, P.K. and Momteiro, P.J.M. *Concrete: Microstructure, Properties, and Materials.* McGraw-Hill Companies, Columbus, OH, 2006
7. CEB-FIP. *CEB-FIP Model Code 1990: Design Code*. Thomas Telford Ltd., London, UK, 1990
8. ACI Committee 209. “Prediction of Creep, Shrinkage, and Temperature Effects in Concrete

Structures." ACI 209R-92, *ACI Manual of Concrete Practice,* American Concrete Institute, Farmington Hills, MI, 1997, 47 pp.

9. Sakata, K., "Prediction of Concrete Creep and Shrinkage, Creep and Shrinkage of Concrete. *Proceedings, 5th International RILEM Symposium*, Barcelona, Spain, Sept. 1993, pp. 649-654.
10. Bazant, Z.P. and Baweja, S. "Creep and Shrinkage Model for Analysis and Design of Concrete Structures - Model B3." *Materials and Structures*, Vol. 28, No. 6, Jul. 1995, pp. 357-365.
11. Muller, H.S., and Hilsdorf, H.K. *Evaluation of the Time-Dependent Behavior of Concrete, Summary Report on the Work of General Task Group 9*. CEB Information Bulletin, No. 199, Sept. 1990, 290 pp.
12. Gardner, N. J. and Lockman, M. J. "Design Provisions for Drying Shrinkage and Creep of Normal-Strength Concrete." *ACI Materials Journal*, Vol. 98, No. 2, Mar.-Apr. 2001, pp. 159-167.
13. ASTM. " ASTM C 403: Standard Test Method for Time of Setting of Concrete Mixture by Penetration Resistance." *Annual Book of ASTM Standards,* American Society for Testing and Materials. West Conshohocken, PA, 1996.
14. AASHTO TP 60-00. "Standard Test Method for the Coefficient of Thermal Expansion of Hydraulic Cement Concrete." *Standard Specifications for Transportation Materials and Methods of Sampling and Testing*, American Association of State Highway and Transportation Officials, Washington, DC, 2004.
15. Jeong J.H. and Zollinger D.G. "Early-Age Curling and Warping Behavior: Insights from a Fully Instrumented Test-Slab System." *Transportation Research Record 1896*, Transportation Research Board, Washington, DC, 2004, pp. 66-74.
16. Jeong J.H. and Zollinger D.G. "Environmental Effects on the Behavior of Jointed Plain Concrete Pavements." *Journal of Transportation Engineering*, ASCE, 2005, Vol. 131, No. 2, pp. 140-148.